Hindawi Publishing Corporation
Journal of Nanomaterials
Volume 2014, Article ID 291273, 7 pages
http://dx.doi.org/10.1155/2014/291273

Research Article

Hydrothermal Synthesis and Hydrogen Sensing Properties of Nanostructured SnO_2 with Different Morphologies

Weigen Chen,[1] Hongli Gan,[1] Wei Zhang,[2] and Zeyu Mao[1]

[1] *State Key Laboratory of Power Transmission Equipment & System Security and New Technology, Chongqing University, Chongqing 400030, China*
[2] *Key Laboratory of Multi-Scale Manufacturing Technology, Chongqing Institute of Green and Intelligent Technology, Chinese Academy of Sciences, Chongqing 400714, China*

Correspondence should be addressed to Hongli Gan; hongligan@foxmail.com and Wei Zhang; zhangwei@cigit.ac.cn

Received 20 February 2014; Revised 1 May 2014; Accepted 15 May 2014; Published 15 June 2014

Academic Editor: Wen Zeng

In this work, nanoscale SnO_2 with various geometrical morphologies, including pine needle-like, sphere-like, sheet-like, grape-like nanostructures, was prepared via a facile hydrothermal process. Microstructures and morphologies of all the as-synthesized products were characterized by X-ray diffraction (XRD) and field emission scanning electron microscopy (FESEM). Meanwhile, the specific surface areas of the as-prepared SnO_2 nanostructures were determined by Brunauer-Emmett-Teller (BET) analysis. Gas sensors were fabricated and their gas sensing properties towards hydrogen were systematically investigated. The results indicate pine needle-like SnO_2 structure exhibits exclusive better gas sensing performances to hydrogen than the other morphologies, which can be attributed to its novel shape with a large specific surface area. Such an unexpected morphology is a promising candidate for the use of SnO_2 as a gas sensing material in future hydrogen sensor applications.

1. Introduction

As important fundamental materials, metal oxides such as ZnO [1, 2], CuO [3], WO_3 [4, 5], and SnO_2 [6–8] have attracted a remarkable interest due to their unique physico-chemical properties. Among them, the n-type large gap semiconductor SnO_2 has been extensively applied in the field of catalysts [9], Li-ion batteries [10], solar cells [11], and gas sensors [12–14]. It is well known that factors such as morphology, crystal structure, and grain size, as well as synthesis method can dramatically affect the gas sensing properties of SnO_2-based sensor [15–19]. Among these factors, the fabrication of well-defined morphology is of great interest and significance to enhance the sensing characteristics of SnO_2 gas sensors for the past few years. Various SnO_2 nanoarchitectures with special morphologies including nanorods [20], nanoflowers [21], nanosheets [22], nanocubes [23], and nanowires [24] have been successfully synthesized via different methods. Indeed, these structures have showed good sensitivity and selectivity to inflammable or toxic gases, such as C_2H_5OH, CO, H_2S, or NO_2. However, up to now, little attention has been paid to the effect of different SnO_2 morphologies on the H_2 gas sensing performances. To date, a variety of methods have been employed to prepare nanocrystalline SnO_2, for instance, sol-gel process [25], chemical vapor deposition [26], coaxial electrospinning [27], and hydrothermal reaction [28]. Compared to other techniques, hydrothermal approach is often adopted for its obvious advantages of simplicity, mild fabrication condition, high purity of product, and low cost [28–30].

In this work, several types of SnO_2 nanomaterials with different morphologies were successfully prepared through an environmentally friendly hydrothermal route. Furthermore, sensing properties of the sensors based on the samples, such as sensitivity, optimum operating temperature, response and recovery times as well as the long-term stability, were systematically tested and compared with each other. The pine needle-like SnO_2 displays better sensitivity, lower working temperature, and more rapid response-recovery time to H_2 than that of the other samples, which implies that the gas sensing properties of SnO_2 sensors can be highly enhanced by preparing SnO_2 with desired morphology.

2. Experimental

2.1. Materials Synthesis. All the reagents purchased from Chongqing Chuandong Chemical Reagent Co., Ltd. were of analytical grade and used as received without any further purification.

Pine needle-like, sphere-like, sheet-like, and grape-like SnO_2 were realized by the hydrothermal synthesis route [28–30].

(a) Pine needle-like SnO_2 structures were prepared as follows: in a typical experiment, 0.05 g $Na_2SnO_3{\cdot}3H_2O$ and 0.02 g NaOH were dissolved into 40 mL deionized water with vigorous stirring for 10 min, and then 0.03 g HMT was added. After the complete dissolution, the precursor was transferred to a Teflon-lined stainless steel autoclave of 50 mL volume and kept at 180°C for 24 h.

(b) Synthesis of SnO_2 nanospheres: 4.0 mmol $SnCl_2{\cdot}2H_2O$ and 10 mmol $Na_3C_6H_5O_7{\cdot}2H_2O$ were mixed together in 20 mL distilled water and stirred for 5 min. 0.02 mmol NaOH was then added to the above solution with continuous stirring to form a homogeneous solution, which was finally transferred to a 25 mL Teflon-lined stainless steel autoclave and heated at 180°C for 12 h.

(c) SnO_2 nanosheets were synthesized as the following process, in which, 0.09 g $SnCl_2{\cdot}2H_2O$, 0.15 g $Na_3C_6H_5O_7{\cdot}2H_2O$, and 0.05 g NaOH were added into 40 mL basic mixture of ethanol and water (1 : 1, v/v) with intense magnetic stirring over 30 min. The reaction mixture was transferred into a 50 mL Teflon-lined stainless steel autoclave at 180°C in 12 h.

(d) The fabrication of grape-like SnO_2 structures is as follows. In a typical procedure, 0.4 g $SnCl_4{\cdot}5H_2O$ was added into NaOH solution (0.5 g, 20 mL). After stirring for 5 min, 30 mmol HMT was added into above solution under vigorous stirring. Then, 20 mL of absolute ethanol was dropwise added to obtain a white translucent suspended solution. Transfer the well-mixed solution into a 50 mL stainless steel autoclave at 180°C for 24 h.

All the above heating autoclaves were cooled to room temperature naturally. The obtained precipitates were retrieved by centrifugation, and then washed several times with distilled water and anhydrous ethanol to remove any possible residues. Finally, all the samples were dried in air at 60°C for about 12 h for further characterizations.

2.2. Fabrication of Gas Sensor. The detailed fabrication of a side-heated gas sensor was as follows: first, each of the above as-synthesized samples was mixed with diethanolamine and ethanol to form a homogeneous paste and then coated onto an alumina tube on which a pair of Au electrodes was previously printed; later, a Ni-Cr heating wire was inserted into the tube for adjusting the operating temperature of the sensor. Finally, all the as-prepared sensors were aged at 300°C for 120 h to enhance their stability and repeatability. The schematic diagram of the gas sensor is shown in Figure 1.

2.3. Characterization and Measurement of Gas Sensing Properties. The crystalline structures of the prepared samples were identified by X-ray diffraction (XRD) with a Rigaku D/Max-1200X diffractometer employing Cu Kα radiation (40 kV, 200 mA and λ = 1.5418 Å). The general morphologies and microstructures were characterized by a Nova 400 Nano field emission scanning electron microscopy (FESEM, FEI, Hillsboro, OR, USA) operated at 5 kV. Meanwhile, the specific surface areas of the products were estimated using the single point Brunauer-Emmett-Teller (BET) method by the 3H-2000 nitrogen adsorption apparatus.

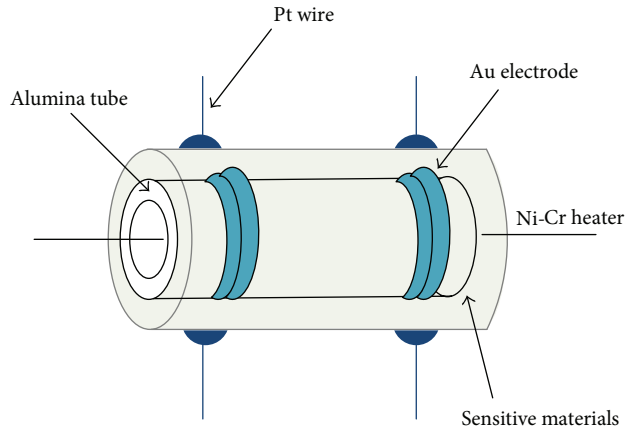

Figure 1: The schematic diagram of the gas sensor.

Gas sensing properties were measured by the chemical gas sensor-8 temperature pressure (CGS-8TP) intelligent gas sensing analysis system (Beijing Elite Tech Co., Ltd). It is convenient to gain parameters for sensor resistance, sensitivity, environmental temperature, and operating temperature, as well as relative humidity from the analysis system. All the sensors needed to be preheated at different operating temperatures for about 30 min. When the sensor resistance value kept steady, a certain concentration of target gas was then injected into the test chamber through a microinjector. The tested gas and air were mixed together using two fans of the analysis system. After the resistance of the sensor attained a new stable value, the test chamber was opened to recover the sensor. The whole experiment process was carried out at constant environment temperature and relative humidity. Repeat all the measurements a few times to ensure the reproducibility of the gas sensing response.

The gas response in this paper was defined as the ratio of sensor resistance in dry air to that in tested gases [31]. The response and recovery times were expressed as the time taken by the sensor to achieve 90% of the total resistance change in the case of adsorption and desorption, respectively [32, 33].

3. Results and Discussion

3.1. Structural and Morphological Characteristics. Figure 2 presents the XRD patterns from the final SnO_2 products. All diffraction peaks are well in accordance with the tetragonal rutile SnO_2 structure (JCPDS file number 41-1445); no other crystal phases and any characteristic peaks from the impurities are observed, confirming that all the samples are of high

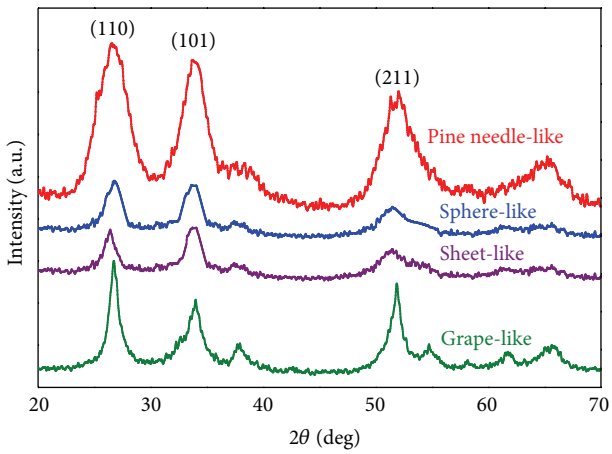

FIGURE 2: XRD patterns of all the SnO_2 samples.

purity and crystallinity. In addition, pine needle-like SnO_2 has broader peaks in comparison with other samples, which demonstrates that the pine needle-like sample has smaller crystal size. BET analysis results indicate that the surface area of pine needle-like, sphere-like, sheet-like, and grape-like was about 30.4 $m^2 g^{-1}$, 21.3 $m^2 g^{-1}$, 20.8 $m^2 g^{-1}$, and 18.2 $m^2 g^{-1}$, respectively. Clearly, pine needle-like SnO_2 possesses much higher specific surface area as compared to other samples. Generally, larger surface area means more active sites and diffusion pathways for gas exchange, which may lead to a larger response.

To gain insight into the detailed morphology of SnO_2 products, typical FESEM images of all the samples can be observed in Figure 3. From Figure 3(a), numerous SnO_2 nanoparticles with smooth surface are clearly observed. They are uniformly distributed and have a nearly spherical morphology with average diameter of 350 nm. As seen in Figure 3(b), the sample contains a large scale of pine needle-like leaves which are well arranged and rather uniform in shape and size. These thin leaves are about 400–500 nm in length and 50–80 nm in width. No other morphologies could be detected, suggesting a high yield of these nanostructures. To the best of our knowledge, such unique shape has not been reported so far, and it may have an obvious influence on promoting gas sensing performances of SnO_2. Figure 3(c) exhibits SnO_2 with grape-like structures assembled from dozen of rugged spheres. Figure 3(d) presents a panoramic image of the SnO_2 sample that consisted of randomly arranged nanosheets and some unshaped nanosheets which are growing.

3.2. H_2 Sensing Properties. Operating temperature is an important fundamental characteristic of gas sensors for its significant impact on sensor response. Figure 4 describes the response curves of these sensors to 200 ppm of H_2 as a function of temperature from 220 to 480°C with an interval of 20°C. Apparently, the responses of the sensors increase with a raise of temperature and reach the maximum and then decrease with further increase of working temperature. Usually, operating temperature of the oxide semiconductor sensor depends on two parameters: electron density of the sensor and reaction rate coefficient between H_2 molecules and adsorbed oxygen species [34]. On one hand, they both increase as the temperature rises. On the other hand, gas response is proportional to reaction rate coefficient but inversely proportional to electron density. Therefore, there should be an optimal temperature to balance the two parameters for achieving the maximum sensor response. In contrast, SnO_2 sensors using samples of pine needle-like, sphere-like, and sheet-like are more sensitive to H_2 than that of grape-like at the same temperature. The highest gas response for pine needle-like, sphere-like, sheet-like, and grape-like SnO_2 was about 20.5, 18, 17, and 14 at temperature of 360°C, 380°C, 380°C, and 400°C, respectively. Herein, the optimal operating temperatures were determined to further examine the characteristics of the sensors. Furthermore, the higher response of pine needle-like SnO_2 probably results from its very fine grain size and large specific surface area.

Figure 5 shows the correlation between the response of SnO_2 sensors and H_2 gas concentrations, where the sensors worked at their own optimum operating temperature as mentioned above. From the curves, it is evident that the response of the sensors increases nonlinearly with no sign of saturation when H_2 concentration ranges from 100 to 1000 ppm. This usually is explained through the gas-diffusion theory by which the oxide based sensor response can be written as $S = aC^b + 1$ [34, 35]. In the formula, a is a controllable constant, b is a charge parameter which reflects oxygen ion species on the surface of SnO_2 sensors, and C is the concentration of the tested gas. Normally, b has value of 1 for O^- and 0.5 for O^{2-}. Besides, it is necessary to know that the growth trends are gradually slowed down with a further rise of gas concentrations. The corresponding data is not presented. This phenomenon might be owing to both the change of stoichiometry about the elementary reactions and the competitions of gas molecules for reaction sites as gas concentrations increase progressively [36, 37]. Specifically, the SnO_2 sensor with pine needle-like structure shows relatively higher sensitivity to H_2 than that of other sensors.

The response and recovery characteristics were studied with the sensors being orderly exposed to 200 ppm of H_2 gas at their own optimum operating temperature, and the curves are depicted in Figure 6. The response and recovery times for the pine needle-like, sphere-like, sheet-like, and grape-like SnO_2 were estimated to be 19–22 s, 22–26 s, 24–27 s, and 25–29 s, respectively. Interestingly, it seems that voltages of all the samples increase dramatically when H_2 is in but go back to their original states when the gas is out. Comparing with the other three SnO_2 nanostructures, it could be noted that the pine needle-like SnO_2 has the shortest response and recovery times, reflecting its excellent sensing performance once again.

Figure 7 displays the long-term stability of the sensors to 200 ppm of H_2 at their own optimum operating temperature with relative humidity of 35%. It could be known that gas response changed slightly after a month, suggesting that all the sensors have good stability and repeatability.

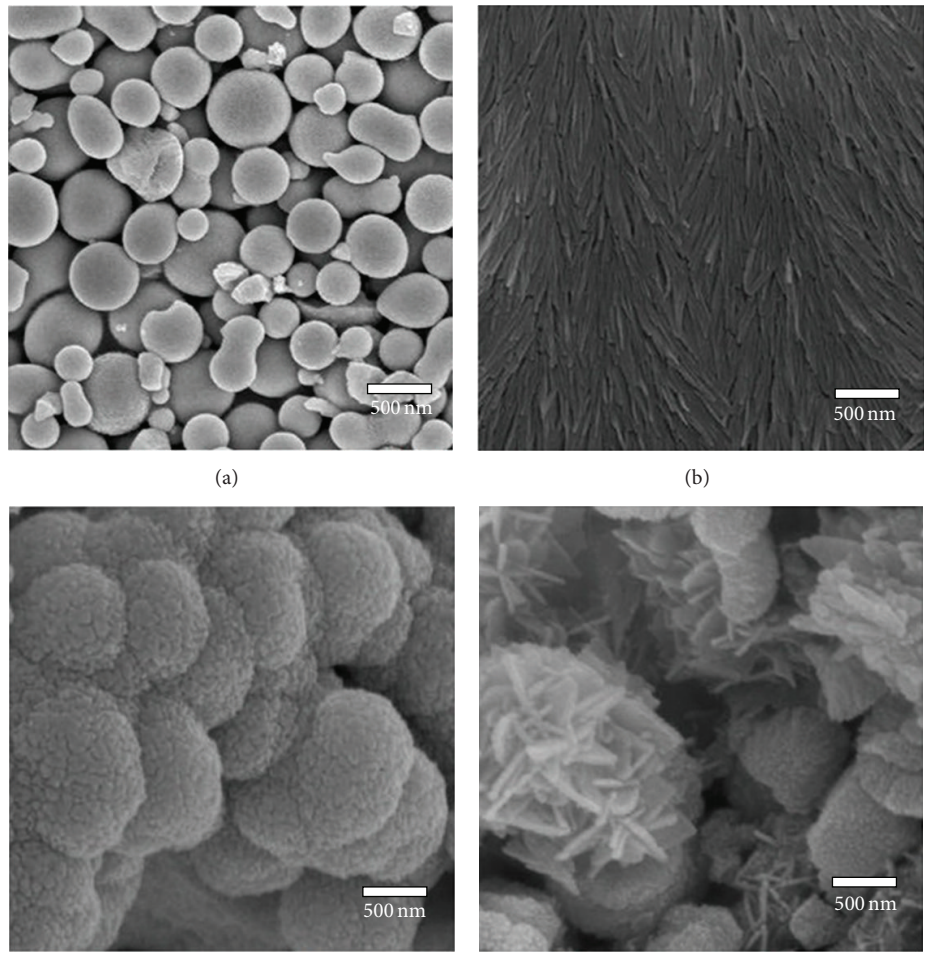

Figure 3: FESEM images of (a) sphere-like, (b) pine needle-like, (c) grape-like, and (d) sheet-like SnO_2.

On the basis of above discussions, one can draw a conclusion that pine needle-like SnO_2 exhibits the most superior sensing properties to H_2 among the four samples.

3.3. Gas Sensing Mechanism. It is believed that the gas sensing mechanism of SnO_2 sensors follows the surface charge model. When sensors contact with different gases, the resistance would have a change. Both the species and amount of oxygen ions play crucial roles in the variation of resistance. When the sensors are exposed to air, oxygen molecules adsorbed on the surface of SnO_2 nanostructures would be ionized to O^{2-}, O^-, or $O_2{}^-$ by capturing free electrons from the conduction band of SnO_2, which causes a depletion layer and consequently increases the resistance of the sensors. As a reducing gas such as H_2 is introduced, chemical reactions between the H_2 molecules and the ionized oxygen are active. This process releases the trapped electrons back to the SnO_2 surface and thus leads to an increase in the carrier concentration and carrier mobility of SnO_2. The gas sensing reaction process on the SnO_2 surface is seen in Figure 8.

The possible reactions involved in the above process are expressed as follows [38, 39]:

$$\begin{aligned}
&O_2\,(\text{gas}) \longrightarrow O_2\,(\text{ads})\\
&O_2\,(\text{ads}) + e^- \longrightarrow O_2{}^-\,(\text{ads})\\
&O_2\,(\text{ads}) + 2e^- \longrightarrow 2O^-\,(\text{ads})\\
&O_2\,(\text{ads}) + 4e^- \longrightarrow 2O^{2-}\,(\text{ads})\\
&H_2\,(\text{gas}) \longrightarrow H_2\,(\text{ads})\\
&H_2\,(\text{ads}) + O^-\,(\text{ads}) \longrightarrow H_2O\,(\text{ads}) + e^-\\
&H_2\,(\text{ads}) + O^{2-}\,(\text{ads}) \longrightarrow H_2O\,(\text{ads}) + 2e^-
\end{aligned} \tag{1}$$

In this experiment, the different sensing properties of the four SnO_2 samples toward H_2 can be ascribed to the different morphologies and nanostructures. Moreover, the higher sensitivity of pine needle-like SnO_2 is mainly based on its special structure with a large surface area which can

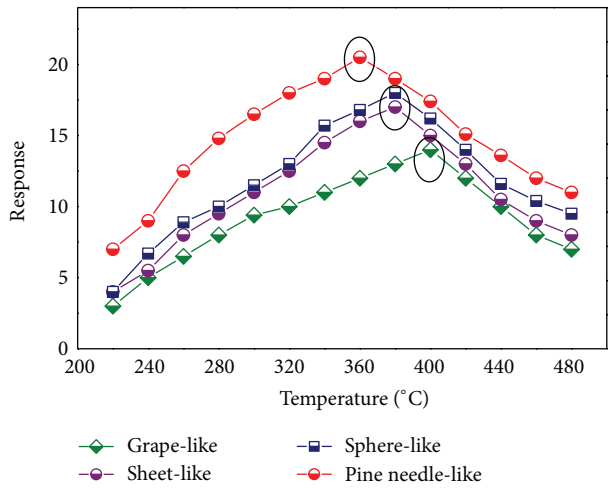

Figure 4: Response of the sensors to 200 ppm of H_2 with different operating temperature (room temperature at 25°C and relative humidity as 35%).

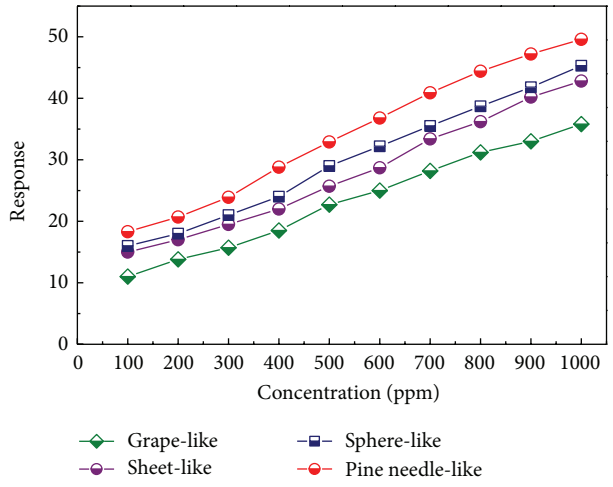

Figure 5: Response of the sensors as a function of H_2 gas concentrations (room temperature at 25°C and relative humidity as 35%).

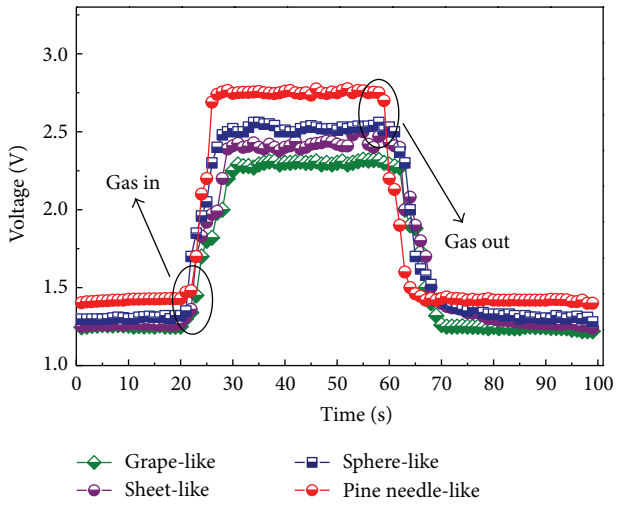

Figure 6: Response-recovery curves of the sensors to 200 ppm of H_2 (room temperature at 25°C and relative humidity as 35%).

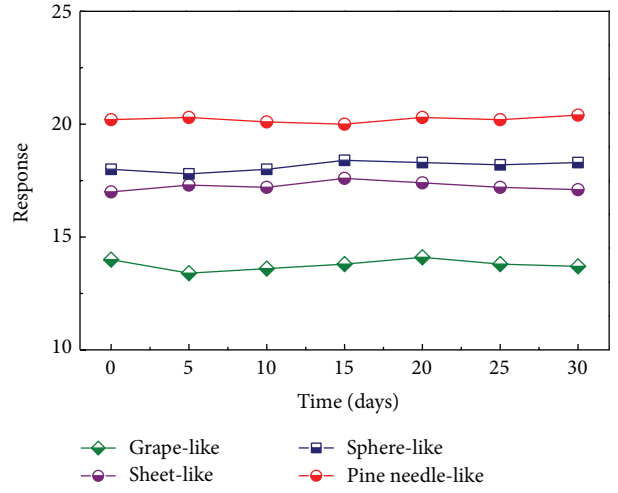

Figure 7: The long-term response value of the sensors to 200 ppm of H_2 (room temperature at 25°C and relative humidity as 35%).

provide more active sites and quick passages for gas exchange and thus enhance the interaction between SnO_2 surface and H_2 molecules.

4. Conclusions

In summary, SnO_2 nanostructures with various morphologies including pine needle-like, sphere-like, sheet-like, and grape-like were realized by hydrothermal preparation. Additionally, both their microstructures and gas sensing properties to H_2 were tested. As compared to other three sensors, pine needle-like SnO_2 sensor exhibits more excellent performances in terms of higher response, faster response-recovery time, and lower working temperature. The good sensing properties may be attributed to the novel pine needle-like structure which has a large specific surface area with massive gas-diffusion channels. The obtained results indicate

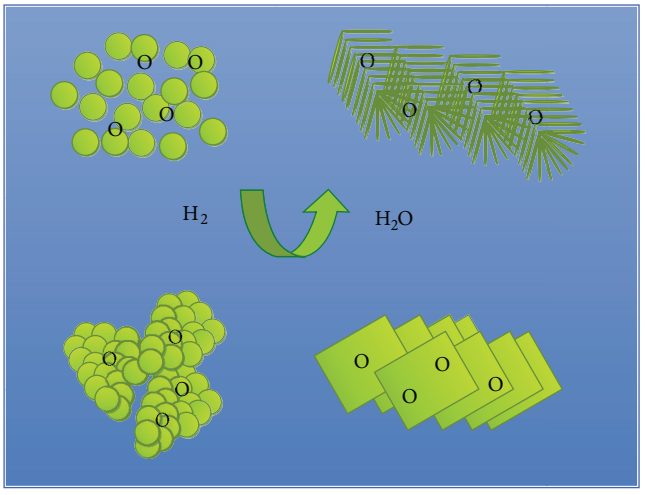

Figure 8: Schematic of the H_2 sensing reaction process.

that the gas sensing properties of SnO_2 sensing materials can be significantly improved by tailoring their surface structures and shapes. These findings offer new opportunities for designing and developing high-performance H_2 gas sensors.

Conflict of Interests

The authors declare that there is no conflict of interests regarding the publication of this paper.

Acknowledgments

The authors appreciate the financial support of the National Natural Science Foundation of China (nos. 51277185 and 51202302), and National Special Fund for Major Research Instrumentation Development (no. 2012YQ16000705).

References

[1] P. Rai, Y.-S. Kim, H.-M. Song, M.-K. Song, and Y.-T. Yu, "The role of gold catalyst on the sensing behavior of ZnO nanorods for CO and NO_2 gases," *Sensors and Actuators B: Chemical*, vol. 165, no. 1, pp. 133–142, 2012.

[2] L. Zhang, J. Zhao, J. Zheng, L. Li, and Z. Zhu, "Hydrothermal synthesis of hierarchical nanoparticle-decorated ZnO microdisks and the structure-enhanced acetylene sensing properties at high temperatures," *Sensors and Actuators B: Chemical*, vol. 158, no. 1, pp. 144–150, 2011.

[3] D. Gopalakrishna, K. Vijayalakshmi, and C. Ravidhas, "Effect of annealing on the properties of nanostructured CuO thin films for enhanced ethanol sensitivity," *Ceramics International*, vol. 39, no. 7, pp. 7685–7691, 2013.

[4] J.-Y. Leng, X.-J. Xu, N. Lv, H.-T. Fan, and T. Zhang, "Synthesis and gas-sensing characteristics of WO_3 nanofibers via electrospinning," *Journal of Colloid and Interface Science*, vol. 356, no. 1, pp. 54–57, 2011.

[5] X. Liu, J. Zhang, T. Yang, X. Guo, S. Wu, and S. Wang, "Synthesis of Pt nanoparticles functionalized WO_3 nanorods and their gas sensing properties," *Sensors and Actuators B: Chemical*, vol. 156, no. 2, pp. 918–923, 2011.

[6] Y. J. Chen, X. Y. Xue, Y. G. Wang, and T. H. Wang, "Synthesis and ethanol sensing characteristics of single crystalline SnO_2 nanorods," *Applied Physics Letters*, vol. 87, Article ID 233503, 2005.

[7] M. Wu, W. Zeng, Q. He, and J. Zhang, "Hydrothermal synthesis of SnO_2 nanocorals, nanofragments and nanograss and their formaldehyde gas-sensing properties," *Materials Science in Semiconductor Processing*, vol. 16, no. 6, pp. 1495–1501, 2013.

[8] J. Liu, X.-C. Tang, Y.-H. Xiao, H. Jia, M.-L. Gong, and F.-Q. Huang, "Porous sheet-like and sphere-like nano-architectures of SnO_2 nanoparticles via a solvent-thermal approach and their gas-sensing performances," *Materials Science and Engineering B: Solid-State Materials for Advanced Technology*, vol. 178, no. 18, pp. 1165–1168, 2013.

[9] I. T. Weber, A. Valentini, L. F. D. Probst, E. Longo, and E. R. Leite, "Catalytic activity of nanometric pure and rare earth-doped SnO_2 samples," *Materials Letters*, vol. 62, no. 10-11, pp. 1677–1680, 2008.

[10] X. W. Lou, Y. Wang, C. Yuan, J. Y. Lee, and L. A. Archer, "Template-free synthesis of SnO_2 hollow nanostructures with high lithium storage capacity," *Advanced Materials*, vol. 18, no. 17, pp. 2325–2329, 2006.

[11] Y. Fukai, Y. Kondo, S. Mori, and E. Suzuki, "Highly efficient dye-sensitized SnO_2 solar cells having sufficient electron diffusion length," *Electrochemistry Communications*, vol. 9, no. 7, pp. 1439–1443, 2007.

[12] W. G. Chen, Q. Z. Li, H. L. Gan et al., "Study of CuO-SnO_2 heterojunction nanostructures for enhanced CO gas sensing properties," *Advances in Applied Ceramics*, vol. 113, no. 3, pp. 139–146, 2014.

[13] M. A. Andio, P. N. Browning, P. A. Morris, and S. A. Akbar, "Comparison of gas sensor performance of SnO_2 nanostructures on microhotplate platforms," *Sensors and Actuators B: Chemical*, vol. 165, no. 1, pp. 13–18, 2012.

[14] Q. Yu, K. Wang, C. Luan, Y. Geng, G. Lian, and D. Cui, "A dual-functional highly responsive gas sensor fabricated from SnO_2 porous nanosolid," *Sensors and Actuators B: Chemical*, vol. 159, no. 1, pp. 271–276, 2011.

[15] G. Zhang and M. Liu, "Effect of particle size and dopant on properties of SnO_2-based gas sensors," *Sensors and Actuators B: Chemical*, vol. 69, no. 1, pp. 144–152, 2000.

[16] R. K. Mishra and P. P. Sahay, "Synthesis, characterization and alcohol sensing property of Zn-doped SnO_2 nanoparticles," *Ceramics International*, vol. 38, no. 3, pp. 2295–2304, 2012.

[17] S. Dai and Z. Yao, "Synthesis of flower-like SnO_2 single crystals and its enhanced photocatalytic activity," *Applied Surface Science*, vol. 258, no. 15, pp. 5703–5706, 2012.

[18] N. Talebian and F. Jafarinezhad, "Morphology-controlled synthesis of SnO_2 nanostructures using hydrothermal method and their photocatalytic applications," *Ceramics International*, vol. 39, no. 7, pp. 8311–8317, 2013.

[19] L. Fei, Y. Xu, Z. Chen et al., "Preparation of porous SnO_2 helical nanotubes and SnO_2 sheets," *Materials Chemistry and Physics*, vol. 140, no. 1, pp. 249–254, 2013.

[20] S. Supothina, R. Rattanakam, S. Vichaphund, and P. Thavorniti, "Effect of synthesis condition on morphology and yield of hydrothermally grown SnO_2 nanorod clusters," *Journal of the European Ceramic Society*, vol. 31, no. 14, pp. 2453–2458, 2011.

[21] J. Huang, K. Yu, C. Gu et al., "Preparation of porous flower-shaped SnO_2 nanostructures and their gas-sensing property," *Sensors and Actuators B: Chemical*, vol. 147, no. 2, pp. 467–474, 2010.

[22] P. Sun, Y. Cao, J. Liu, Y. Sun, J. Ma, and G. Lu, "Dispersive SnO_2 nanosheets: hydrothermal synthesis and gas-sensing properties," *Sensors and Actuators B: Chemical*, vol. 156, no. 2, pp. 779–783, 2011.

[23] L. Yu, M. Zhang, Y. J. Chen et al., "Assembling SnO_2 nanocubes to nanospheres for high-sensitivity sensors," *Solid State Sciences*, vol. 14, no. 4, pp. 522–527, 2012.

[24] G. D. Zhang and N. Liu, "A novel method for massive synthesis of SnO_2 nanowires," *Bulletin of Materials Science*, vol. 36, no. 6, pp. 953–960, 2013.

[25] M. A. Dal Santos, A. C. Antunes, C. Ribeiro et al., "Electric and morphologic properties of SnO_2 films prepared by modified sol-gel process," *Materials Letters*, vol. 57, no. 28, pp. 4378–4381, 2003.

[26] J. B. Zhang, X. N. Li, S. L. Bai, R. X. Luo, A. F. Chen, and Y. Lin, "High-yield synthesis of SnO_2 nanobelts by water-assisted chemical vapor deposition for sensor applications," *Materials Research Bulletin*, vol. 47, no. 11, pp. 3277–3282, 2012.

[27] Y. Zhang, J. Li, G. An, and X. He, "Highly porous SnO_2 fibers by electrospinning and oxygen plasma etching and its ethanol-sensing properties," *Sensors and Actuators B: Chemical*, vol. 144, no. 1, pp. 43–48, 2010.

[28] W. G. Chen, Q. Zhou, and S. D. Peng, "Hydrothermal synthesis of Pt-, Fe-, and Zn-doped SnO_2 nanospheres and carbon monoxide sensing properties," *Advances in Materials Science and Engineering*, vol. 2013, Article ID 578460, 8 pages, 2013.

[29] Y. L. Wang, M. Guo, M. Zhang, and X. D. Wang, "Facile synthesis of SnO_2 nanograss array films by hydrothermal method," *Thin Solid Films*, vol. 518, no. 18, pp. 5098–5103, 2010.

[30] B. Mehrabi Matin, Y. Mortazavi, A. A. Khodadadi, A. Abbasi, and A. Anaraki Firooz, "Alkaline- and template-free hydrothermal synthesis of stable SnO_2 nanoparticles and nanorods for CO and ethanol gas sensing," *Sensors and Actuators B: Chemical*, vol. 151, no. 1, pp. 140–145, 2010.

[31] W. G. Chen, Q. Zhou, L. N. Xu et al., "Improved methane sensing properties of Co-doped SnO_2 electrospun nanofibers," *Journal of Nanomaterials*, vol. 2013, Article ID 173232, 9 pages, 2013.

[32] Y. Gui, F. Dong, Y. Zhang, and J. Tian, "Preparation and gas sensitivity of WO_3 hollow microspheres and SnO_2 doped heterojunction sensors," *Materials Science in Semiconductor Processing*, vol. 16, no. 6, pp. 1531–1537, 2013.

[33] Q. Zhou, W. Chen, L. Xu, and S. Peng, "Hydrothermal synthesis of various hierarchical ZnO nanostructures and their methane sensing properties," *Sensors*, vol. 13, no. 5, pp. 6171–6182, 2013.

[34] N. Hongsith, E. Wongrat, T. Kerdcharoen, and S. Choopun, "Sensor response formula for sensor based on ZnO nanostructures," *Sensors and Actuators B: Chemical*, vol. 144, no. 1, pp. 67–72, 2010.

[35] Q. Wan, Q. H. Li, Y. J. Chen et al., "Fabrication and ethanol sensing characteristics of ZnO nanowire gas sensors," *Applied Physics Letters*, vol. 84, no. 18, pp. 3654–3656, 2004.

[36] M. Chen, Z. Wang, D. Han, F. Gu, and G. Guo, "High-sensitivity NO_2 gas sensors based on flower-like and tube-like ZnO nanomaterials," *Sensors and Actuators B: Chemical*, vol. 157, no. 2, pp. 565–574, 2011.

[37] M.-W. Ahn, K.-S. Park, J.-H. Heo, D.-W. Kim, K. J. Choi, and J.-G. Park, "On-chip fabrication of ZnO-nanowire gas sensor with high gas sensitivity," *Sensors and Actuators B: Chemical*, vol. 138, no. 1, pp. 168–173, 2009.

[38] S. Mishra, C. Ghanshyam, R. A. M. Nathai, S. Singh, R. P. Bajpai, and R. K. Bedi, "Alcohol sensing of tin oxide thin film prepared by sol-gel process," *Bulletin of Materials Science*, vol. 25, no. 3, pp. 231–234, 2002.

[39] M. Hübner, R. G. Pavelko, N. Barsan, and U. Weimar, "Influence of oxygen backgrounds on hydrogen sensing with SnO_2 nanomaterials," *Sensors and Actuators B: Chemical*, vol. 154, no. 2, pp. 264–269, 2011.